Chapter - II

Preparation And Characterisation

CHAPTER -II

PREPARATION AND CHARACTERISATION

2.1 INTRODUCTION :

The properties of ferrites are mainly depend on the phisco-chemical state of the materials. The properties of the ferrites can be classified as intrinsic and structure sensitive. The method of preparation needs the heat treatment for the formation of crystal structure, and it also influences the intrinsic properties which are usually understood in terms of cation distribution. However, the details about the heat treatment like firing temperature, time, atmosphere and cooling rate etc, constitute the thermal history of the sample through the imprint on almost all the attendant microstructural factors like defect concentration, porosity, inclusions and orientation, size and shape of the grains, and grain boundaries etc. In ceramic method care has to be taken into account regarding the homogeneity of the material. The ceramic method makes it possible to prepare complex chemical composition, desired microstructure and shapes of the final product much more economical than other methods. The grain growth, densification and microstructural features develop during sintering process.

In this chapter a brief review of the method of preparation, ceramic processes and development of microstructure relating to time

and temperature are discussed. Role of atmosphere which influences the microstructure of ferrites is also discussed. The method of preparation of ferrite samples in our laboratory is given.

SECTION : A

2.2 PREPARATION OF FERRITE :

Generally the ferrites are prepared by the standard ceramic method using oxides and carbonates. As we know the ferrites being the oxide materials, no special extraction or preparation techniques involving molten phases are required. In the preparation, the starting materials and mixtures are allowed to undergo solid state reaction and therefore, it is usually called as ceramic process. A flow of chart is given below in Fig. 2.1.

2.3 METHOD OF PREPARATION OF FERRITES :

The general methods for the preparation of ferrite compositions are given as follows.

a) Oxide method. (b) Decomposition method

c) Hydroxide method. (c) Oxalate method.

2.3 (a) OXIDE METHOD :

This method is most extensively used in the commercial production of ferrites, which requires little chemical knowledge. In this method, oxides with very pure form can be mixed together

Flowchart of the stages in the ferrite preparation.

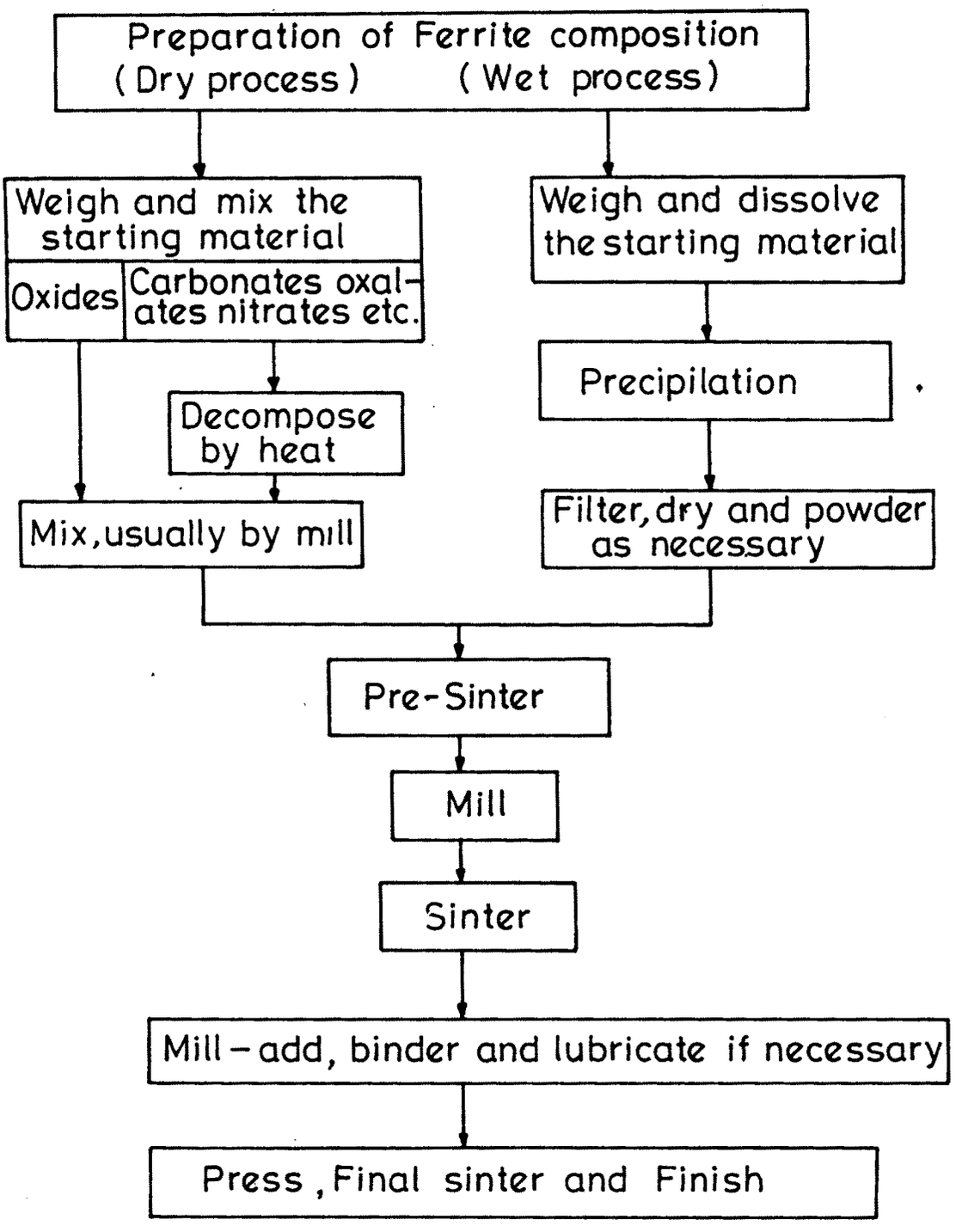

Fig. 2·1

for their final product. They are mixed manually and wet milled with steel balls for few hours. After milling, the dry mixture is passed through the mesh screen. The mixture is then heated at required temperature and slowly cooled to room temperature. The obtained powder is pressed with the help of hydrolic press to a suitable shape and finally sintered at elevated temperature.

2.3 (b) DECOMPOSTION METHOD :

In this method, one may start with carbonates, nitrates and oxalates instead of using oxides. These materials are mixed with required proportions and usually preheated in air which produces oxides by thermal decomposition. The oxide prepared ' in situ' are more readily undergo solid state reaction.[1] The details of this method are similar to oxide method.

2.3 (c) HYDROXIDE PRECIPITATION METHOD :

This method for the preparation of ferrites have been established by Economos.[2] Hydroxide precipitation method is also applied for preparation of YIG.[3] In this method, chemical process must be understood quantitatively in order to ensure the simultaneous precipitation of hydroxides. This method necessarily requires simultaneous precipation otherwise the value of this method is lost. One or both of the precipitation may form in a state which may make filteration difficult, because sodium ions may be absorbed on the precipitate getting ocluded as impurities. Sato[4] and his

co-workers[15] prepared ultrafine spinel ferrites by using this method and studied their properties.

2.3(e) OXALATE PRECIPITATION METHOD :

Precipitation can be carried out by using ammonium oxalate which does not leave any residue after heating. Most of the metal oxalates are nearly similar in crystal structure . so the precipatation produces mixed crystal which contains metallic cations with correct proportions. Therefore, mixing with correct ratio can be obtained on molecular scale. In the technique, if the precipation occurs which are of different rules then they do not form uniformity. Careful heating at elevated temperature of precipitation gives, ferrites with particle size less than 1 μm.

2.4 PRESINTERING AND SINTERING :

When a mixture of raw materials is heated at a temperature round about 650 to 700°C below its final sintering temperature, the process is so called pre-sintering. In this process slow solid state reaction takes place, where the reactant of the raw material partly react so as to form the final product. The rate of solid state reaction depends upon the reactivity of the compounds as well as presintering temperature. The purpose of presintering is used to decompose higher oxides and carbonates which reduces the evaluation of gas in the final sintering process. Secondly it assists in

homogenising of the material. Thirdly it is used to reduce variation in the composition of raw material. Lastly, it is used to control the shrinkage of the material that occurs during final sintering.

In the final sintering process the material achives uniform composition distribution and microstructure development. The microstructure mainly depends on the reactivity of the starting materials and sintering temperature.

2.5 MICROSTRUCTURE AND FERRITE :

The relation between microstructure and properties of ferrites have been discussed by the number of workers. The development of microstructure changs the electrical and magnetic properties of ferrites. Guillaud[6] et al have measured the resistance of Mn-Zn ferrite and observed that the high resistivity in the materials is due to grain boundary resistance as one of the factor. Heister[7] tressed the need of uniform grain size for minimum loss. The structure with large crystallites favour domain wall motion which results in large retentivity and coercivity. Perduijn and other investigators[8], have shown the linear relationship between the permeability and grain diameter.

After final sintering we assume that the cations are present in correct proportions. The object then remains to achive suitable microstructure together with correct oxygen content and the distribution of cations. These are affected by time and temperature of sintering, partial pressure of oxygen and cooling rate. Sintering

consists of heating the powder compact to a temperature at which the mobability is sufficiently high to decrease the free energy associated with grain boundaries During sintering, densification and grain growth occurs and give rise to a variety of microstructure. The driving force for sintering process is obtained from surface energy of particles. The surface energy per unit volume of spherical particle is given by,

$$E_s = \sigma\gamma / D \qquad .....(2.1)$$

where γ- surface tension and D is the diameter of spherical powder particle. Volume diffusion is the main mechanism in ionic solids. Surface diffusion may plays a part in the beginning of the process in the formation of contact area between particles. The surface of pore act as the source of vacancies. Migration of vacancies occurs as a result of concentration between the curved surface of the pores and equilibrium vacancy concentration under the flat surface (Co). The concentration of vacancy under a surface of radias (r) is represented by Kelvin's equation,

$$c(r) = Co \exp (2 \ a^3/rkT) \qquad .....(2.2)$$

Co = is vacancy concentration under flat surface

a^3 = is vacancy volume.

As concentration of grain boundary is equal to 'Co', then the vacancy migrate from pore surface into grain boundaries with temperature.

2.5 (a) NORMAL GRAIN GROWTH :

In grain growth the grain boundary energy is decreased when boundaries move towards their center of curvature. The emperical rate of grain growth is given by,[9]

$$D - D_o = kt^n \qquad .....(2.3)$$

D_o = is original particle size,

t = is time,

k = is temperature dependance factor,

n = is grain growth exponent, usually 1/2 or 1/3.

The presence of impurities in the grain boundaries hinders the grain growth. When pores or inclusions dissappear during heating, the large grain is formed. The grain grwoth occurs until the following condition[10] is satisfied.

$$D_{cr} = d_i/f_i \qquad .....(2.4)$$

D_{cr} = is critical diameter of the grain,

d_i = is diameter of inclusions,

f_i = is volume fraction of inclusions.

2.5 (b) EXAGGERATED GRAIN GROWTH :

The exaggerated grain growth occurs when average grain size reaches the critical size. In this situation few grains grow rapidly at the expense of others due to lack of homogeneity. The discontineous grain growth leads to a duplex structure of joint grains

in a matrix of small grains. The rapid grain growth entraps the pores with in the matrix and it is almost impossible to eliminate such pores due to their large distance from grain boundaries. Lack of chemical homogenity as well as variation in density and presence of impurities favours exaggerated grain growth.

2.6 HOT PRESSING :

Hot pressing means to achieve a dense ferrite material at sufficiently low temperature without grain grwoth. This technique involves simultaneous application of pressure and temperature. The application of pressure makes use of lower sintering temperature. The main factors affecting the hot process are time, temperature, pressure, particle characteristics and environment. Hot pressing is the process for eliminating porosity.

In most analysis of data on hot pressing influence surface energy which is increased. In hot preessing the magnitude of driving force contributed by surface tension is of the order of magnitude that contributed by applied pressure. Hence for evaluation of driving force during densification, the effect of surface energy must be considered. This technique has significant control over the microstructure as a function of pressure, temperature and time and achieves high densification. Recently gas isotatic hot pressing has been described to achieve maximum possible density. Hardt has reported the density more than 99.6% in garnet and spinel ferrite

by this technique.

2.7 SINTERING ATMOSPHERE :

It has been observed that sintering atmosphere plays an important role in sintering process. It must be remembered that Fe_2O_3 content can depend on the degree of oxidation or reduction of ferrite. The reduction of ferric to ferrous ion occurs at high temperature or at low oxygen pressure. The explanation for an effect of dificit Fe_2O_3 was given by Reignen.[11]

In an anion deficient ferrite the principle process where by pores shrink consists of the diffusion of anion vacancies to grain boundaries. In cation deficient ferrites the pores can be pulled along grain boundaries with other pores when they meet by involving oxygen transport via gas phase and the cation vacancies throughout the material surrounding the pore. The cation diffusion is facilitated by cation vacancies.

2.8 ACTUAL PREPARATION OF FERRITE SAMPLES :

The ferrite samples were prepared by usual ceramic method starting with oxides or carbonates. The general formula of composition is given by,

$$Cd_{0.3}\ Ni_{0.7+t}Mn_tFe_{2-2t}\ O_4$$

where t = 0 to 0.4

The molecular weight compositions are given in Table 2.1

TABLE 2.1

COMPOSITIONASL WEIGHTS OF POWDERS.

Variable t	Weight of $CdCO_3$ grams	Weight of NiO grams	Weight of MnO_2 grams	Weight of Fe_2O_3 grams
0.00	2.586	2.615	-	7.985
0.05	2.586	2.802	0.217	7.585
0.10	2.586	2.988	0.435	7.186
0.15	2.586	3.175	0.652	6.787
0.20	2.586	3.362	0.869	6.388
0.30	2.586	3.735	1.304	5.589
0.40	2.586	4.109	1.739	4.791

2.9 MIXING AND PRESINTERING :

A.R.grade carbonates of $CdCO_3$ and oxides of MnO_2, NiO, Fe_2O_3 were weighted in required mole proportions on semimicrobalance (owalabour) and mixed thoroughly in an agate-morter with acetone. This mixture was then taken into platinum crucible and heated at 700^oC for 7 hours in a furnace. The temperature of the furnace was measuremed with the help of calibrated chromel-Alumel thermocouple. The samples were cooled to room temperature by switching off the furnace. The cooling rate was high at higher temperature and low

at lower temperature. The pre sintered samples were again reground in an agate morter with acetone. The fine powder was collected in a clean glass tube.

Few grams of sample was taken into agate morter and P.V.A was used as binder. Then the dry powder was poured into the die having 1 cm in diameter and was kept under the pressure of 8 tonnes with hydraulic press for 5 minutes. Then pellet was taken from the die by removing the load. The toroid was formed by using toroid die about 1.8 cm in outer and 0.8 cm in inner diameter.

2.10 SINTERING :

The pellet and toroid thus prepared were taken on a clean plattinum foil and sintered at $950^{o}C$ for 20 hours in a glow bar furnace. The temperature of the furnace was increased by $100^{o}C$/hours. The furnace was cooled at the rate of $100^{o}C$/hour for first few hours (3 hours) and then nearly $50^{o}C$/hours for intermediate stage upto room temperature. The temperature was measured by Crome-Alumel thermocouple.

SECTION-B

X-RAY DIFFRACTION STUDY.

2.11 INTRODUCTION :

the characterisation of the ferrites can be done by using X-ray diffraction, Neutron diffraction, Mossbour spectroscopy etc. The X-ray diffraction technique is well established tool to study the crystal structure and confirms the formation of solid solution reaction. In order to confirm the formation of ferrite and to determine the lattice parameter of the spinel phase, we have used this tool for the series $Cd_{0.3}Ni_{0.7+t}Mn_tFe_{2-2t}O_4$

2.12 CONDITION FOR X-RAY DIFFRACTION :

The regular three dimensional arrangement of unit cells in the crystal can be regarded as three dimensional diffraction gratting for X-ray. According to Braggs[21] diffraction it is possible only when the wave length of X-ray is comparable with inter planer spacing. The Bragg's law is,

$$2d \sin\theta = n\lambda \qquad .....(2.5)$$

where, d = is the interplaner spacing,

n = is the integral number,

$\theta < \sin\theta < 1 \implies n\lambda < 2nd'$

Since, n = 1 is the least value of 'n' in the diffraction condition, for any observable angle '2 θ'

$$\lambda = 2d' \qquad .....(2.6)$$

Bragg's law can be represented as,

$$\lambda = 2 \frac{d'}{n} \text{ Sin } \theta \qquad \text{.....(2.7)}$$

For convenience, replacing $\frac{d'}{n}$ by d, we get,

$$\lambda = 2 \text{ d Sin } \theta \qquad \text{.....(2.8)}$$

The applicability of the law can be illustrated in Fig.2.2, Fig. (2.2a) represents the 2^{nd} order (100) reflection. If there is no real plane midway between the (100) plane, it can be imagined as in Fig. (2.2b) forming 1^{st} order reflection for adjacent (200) planes.

For the cubic crystal[13] the interplaner distance in (hkl) set of plane is,

$$1/d^2 = (h^2 + k^2 + l^2) / a^2 \qquad \text{.....(2.9)}$$

where, a = is unit cell size,

combining with the Bragg's law, we have,

$$\text{Sin}^2\theta_{hkl} = \lambda^2/4a^2 \ (h^2 + k^2 + l^2) \qquad \text{.....(2.10)}$$

This equation represents the Bragg's angle for diffraction occuring from the plane (hkl) for known values of λ. For tetragonal crystal.[13]

$$\text{Sin}^2\theta_{hkl} = \lambda^2/4 \ (h^2 + k^2) /a^2 + l^2/c^2) \qquad \text{.....(2.11)}$$

where a and c are axes of tetragonal crystal.

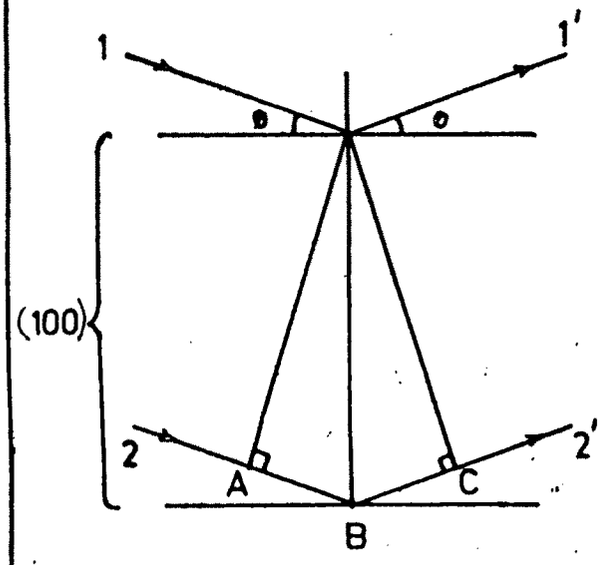

Fig.: 2·2a

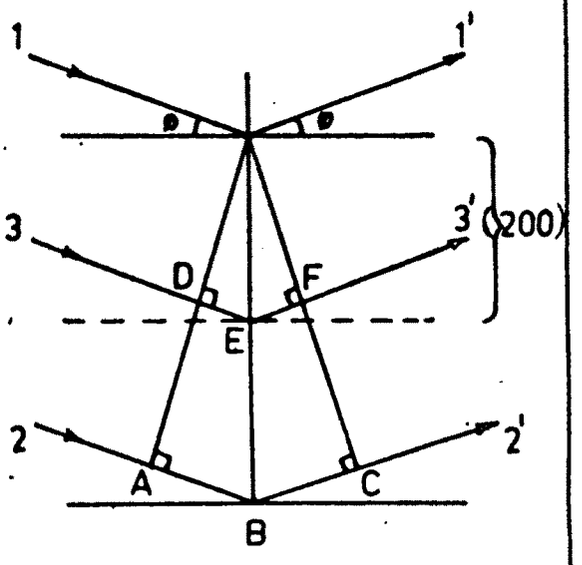

Fig.: 2·2b

The Application of Bragg's Low.

Fig. 2·2

Thus the diffraction direction as predicted by equation 2.10 and 2.11 are determined solely by the shape and size of the unit cell. The converse of this statement is most important as far as crystal analysis is concerned. The intensities of direction of diffracted beam gives the information regarding the positions of atoms for the structural analysis of crystal from diffraction pattern, diffracted angle ' θ ' can be measured. For known values of wavelength λ inter planer distance 'd' can be calculated by Bragg's law as,

$$\lambda = 2d \sin\theta \qquad \ldots(2.12)$$

2.13 EXPERIMENTAL DIFFRACTION METHOD :

The experimental diffraction methods are as follows :

a) Laue method (b) Rotating crystal method

c) Powder method and its principle

d) X-ray diffractometer and its principle.

2.13 (a) POWDER METHOD AND ITS PRINCIPLE :

The method of X-ray diffraction was first developed by P.Debye and P.Scherrer[14] in 1916 and independently by A.W. Hull[15] in 1917. In this method the film is placed on cylindrical surface of Debye Scherrer Camera and specimen holder rotates about the axis of camera in a monoenergetic beam of X-rays. The small amount of powder can be coated on a surface of a fine glass fibre with glue or petroleum jelly. The specimen is then mounted in its holder

by proper adjustment.

The crystallites are randomly oriented so that reciprocal lattice vector of all crystallites are oriented in all the directions. The reciprocal lattice prints lie on the surface of sphere of radicles (hkl) and is oriented by every possible values of hkl cuts the E-wald's sphere Fig. 2.3.

By the geometry of Ewald's sphere,

$$4\,\theta_{hkl} = \frac{S_{hkl}}{R} \qquad .....(2.13)$$

If we consider two consecutive reflections the angle between them is Bragg angle and is given by,

$$\theta_{hkl} = \frac{S_{hkl}}{4} \qquad .....(2.14)$$

The measurements of S_{hkl} is in mm on a photographic film gives the values of θ_{hkl}

Using Bragg's law we have,

$$2d_{hkl} \operatorname{Sin} \theta_{hkl} = \lambda \qquad .....(2.15)$$

The inter-planer spacing d_{hkl} can be determined.

2.13 (b) X-RAY DIFFRACTOMETER AND ITS PRINCIPLE :

The principle of this method and main features are shown in Fig. 2.4. The incident beam of X-ray is allowed to pass through the slit 'A' of the collimeter. As the crystallites are randomly

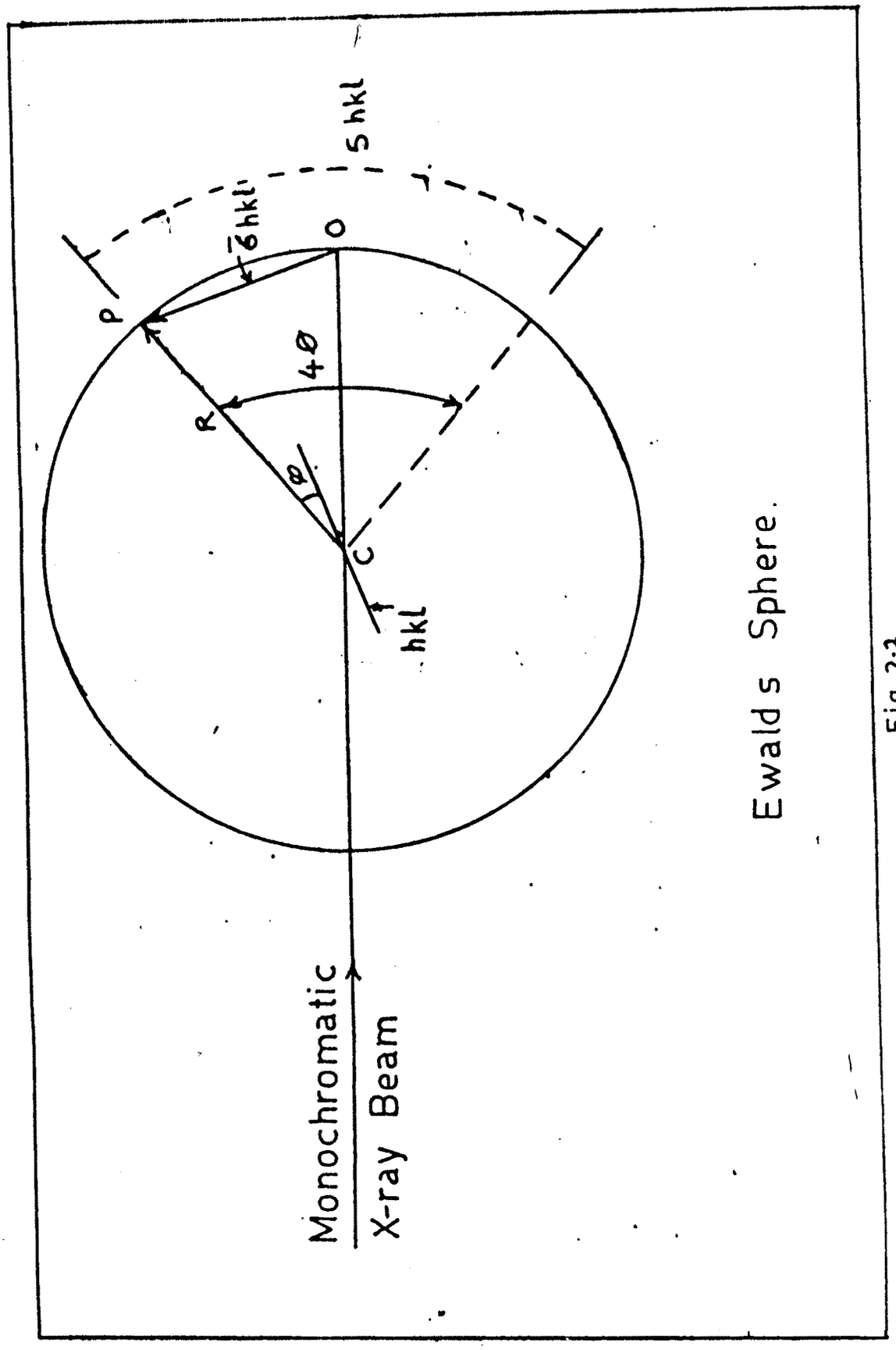
S hkl
O
P
$\bar{S}$ hkl
2θ
R
θ
C
hkl
Monochromatic
X-ray Beam
Ewald s Sphere.

Fig. 2·3

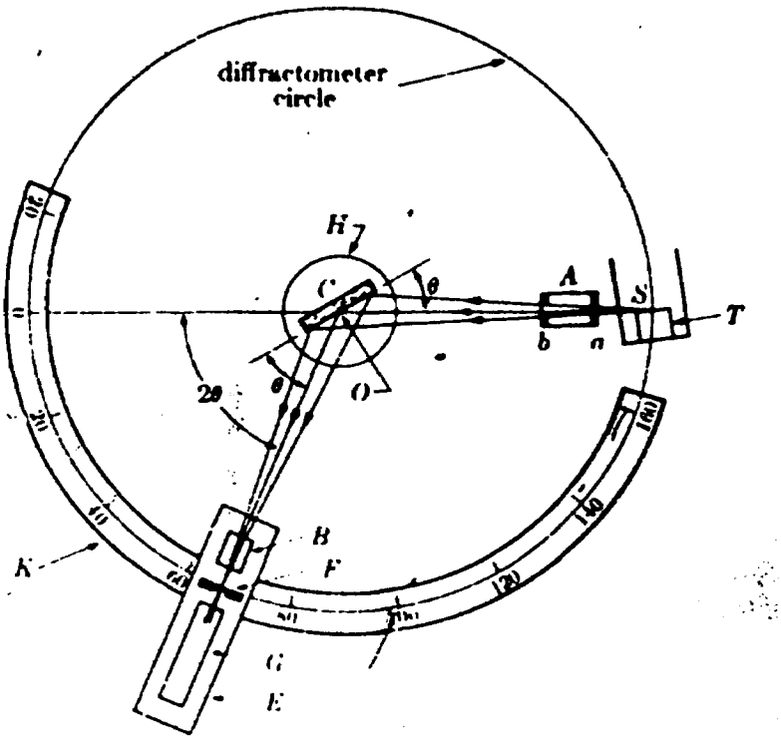

PLATE 2-4 : PRINCIPLE OF THE X-RAY DIFFRACTOMETER

oriented , a reflection at the particular position is due to a set of atomic planes which satisfy Bragg's condition. The diffracted beam gets converged and focused at a slit 'F' which further enters the counter 'G' with the help of special slit B, the diffracted beam is collimated. The counter G is connected to a count rate meter and output of the circuit is fed to a fast automatic recorder which registers counts per second versus 2θ . The location of centroid of the recorded peak gives $2\ \theta_{hkl}$ for corresponding Bragg-reflection.

The receiving slit and counter are supported on the carriage 'E' which can be rotated about the vertical axis through 'C' whose angular position '2θ ' can be read on circular scale 'k', as counter moves through 2θ degree between E and H. It is also ensures that the complementary angle of incidence and reflection from flat specimen are always equal to each other, each being half the total angle of diffraction. This type of arrangement is necessary to satisfy the focusing condition. The power driven counter moves with constant angular velocity about the axis of the diffractometer for any desired angular range from 10^{o} to 160^{o}. The main advantage of the diffractometer over the debye -scherrer powder method is that, it gives a quantitative measure of the intensity.

2.14 EXPERIMENTAL :

The X-ray diffraction of ferrite system $Cd_{0.3}$, $Ni_{0.7+t}$ $Mn_tFe_{2-2t}O_4$ (t= 0 to 0.4) were taken by using philips make p.w. 1051 X-ray diffractometer. The powder was spread uniformly on mounted screen of sample holder so as to form plane surface of the specimen. Copper target was used of which the wavelength of CuKα being 1.5418 A^o. The speed of chart was 1 degree per cm. rotation angle. The recording was made from 10^o to 80^o of 2θ. The reflections were indexed by usual method.

From the chart the values of peaks was recorded and d values were calculated from Brgg's law,

$$2\ d\ \sin\theta = n\ \lambda \qquad .....(2.16)$$

and also by using the relation,

$$d_{cal} = \frac{a}{\sqrt{h^2+k^2+l^2}} \qquad .....(2.17)$$

where a = is lattice constant.

The following equations are used to calculated R_A and R_B values.

$$R_A = (u - 1/4)\ a\ \sqrt{3} \qquad .....(2.18)$$

$$R_B = (5/8 - u)\ a \qquad .....(2.19)$$

where U = 0.381 A^o. Ni ferrite.

2.14(a)INDEXING OF THE POWDER PATTERN :

The powder pattern of each slow cooled sample of $Cd_{0.3}Ni_{0.7+t}Mn_tFe_{2-2t}O_4$ were obtained with the help of diffractometer. The object of scanning was kept over wide range between 10^o to 80^o. The values of $Sin^2\theta$ was calculated for each peak. For cubic structure the relation between the inter planer spacing d_{hkl}, lattice parameter 'a' and indices h,k,l can be given by the formula.[16]

$$d_{hkl} = \frac{a}{\sqrt{h^2+k^2+l^2}} \qquad \ldots.(2.20)$$

As the peak in the diffraction pattern is obtained, the Bragg's law must be obeyed.

$$2\, d_{hkl}\, \text{Sin}\, \theta_{hkl} = \lambda \qquad \ldots..(2.21)$$

combining these two equations,

$$2\, \frac{a}{\sqrt{h^2+k^2+l^2}}\, \text{Sin}\, \theta_{hkl} = \lambda \qquad \ldots..(2.22)$$

$$\frac{\text{Sin}^2\theta_{hkl}}{h^2+k^2+l^2} = \frac{\text{Sin}^2\,\theta_{hkl}}{S} = \frac{\lambda 2}{4a^2} \qquad \ldots..(2.23)$$

where $S = h^2 + k^2 + l^2$

The sum S is always an integer and the term $\lambda^2/4a^2$ must be constant. The value of sum 'S' is selected to yield constant quotient when divided one by one into observed Sin 2θ values. Rearranging the equation (2.23).

$$\sin^2\theta_{hkl} = \lambda^2 S/4a^2 \qquad .....(2.24)$$

The quantity $\lambda^2/4a^2$ is the greatest common factor (GCF) in $\sin^2\theta$ In the first step, G.C.F. was determined from few lines and then all other integers were found. Once the integer 'S; were known, the indices hkl of reflecting planes were written down by inspection. When a set of integers satisfying equation (2.23) were not found, the other possible tetragonal system was checked and found in good agreement.

2.14 (b) SCANNING ELECTRON MICROSCOPY (SEM) :

The micrographs of our series $Cd_{0.3}Ni_{0.7+t}Mn_tFe_{2-2t}O_4$ were taken with the help of SEM (Cembridge steroscan S-250MK III) at R.S.I.C. Nagpur. Initially the pellets were coated with gold. The gold coated samples were then kept inside the steroscan S-250 MKIII. This instrument was on for more than 1/2 hours to attained required vaccume pressure. Then the samples was scanned for various surfaces and photographs were taken of the selected surfaces with the help of camera. The photographic film was developed with the help of developer and fixer. The negatives were used to get the positive photographs. They are shown in Fig. 2.5 to 2.10. With the help of positive photographs, the average grain diameter was calculated.

2.15 RESULTS AND DISCUSSION :

2.15 (a) X-RAY DIFFRATION :

X-ray diffractograms of the series $Cd_{0.3}Ni_{0.7+t}Mn_tFe_{2-2t}O_4$

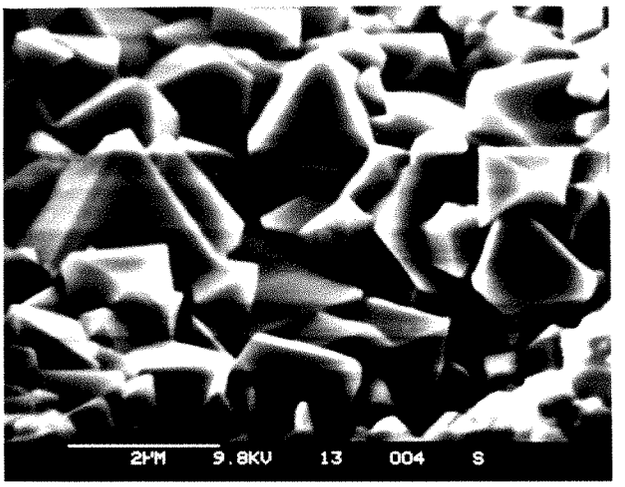

Fig: 2.5

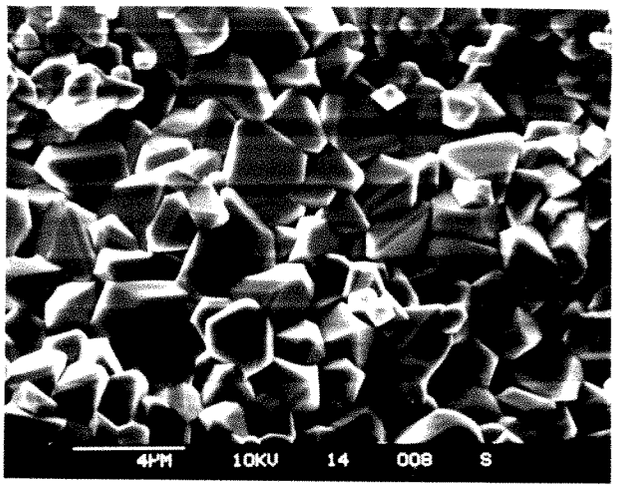

Fig : 2.6

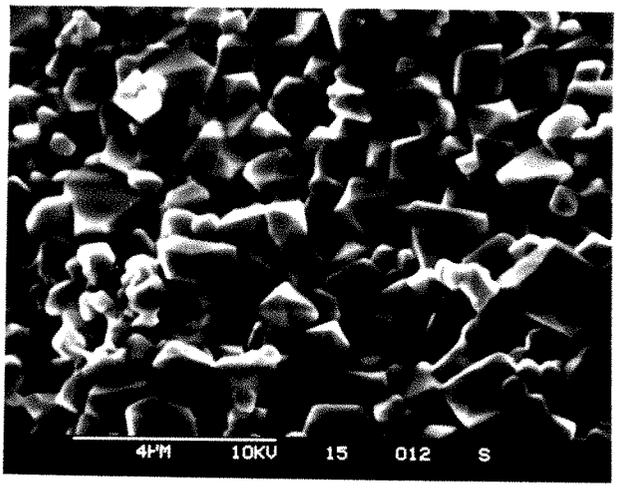

Fig: 2.7

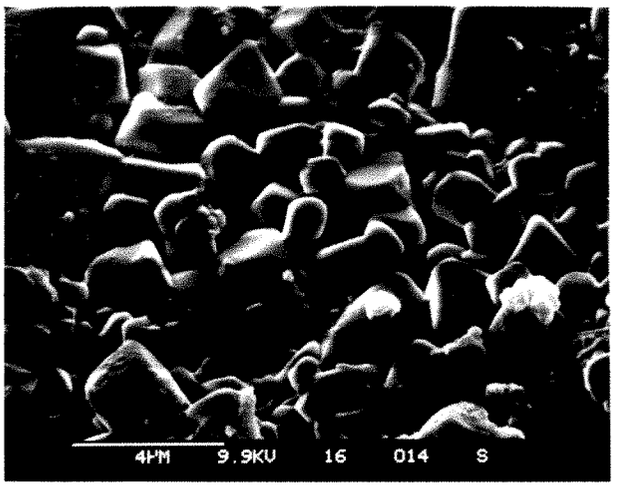

Fig: 2·8

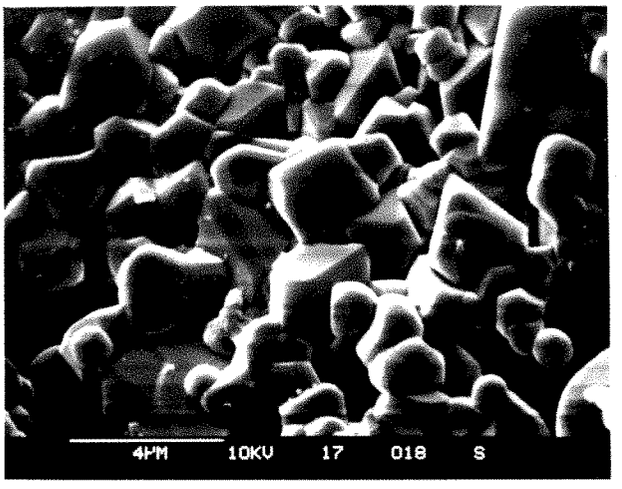

Fig: 2·9

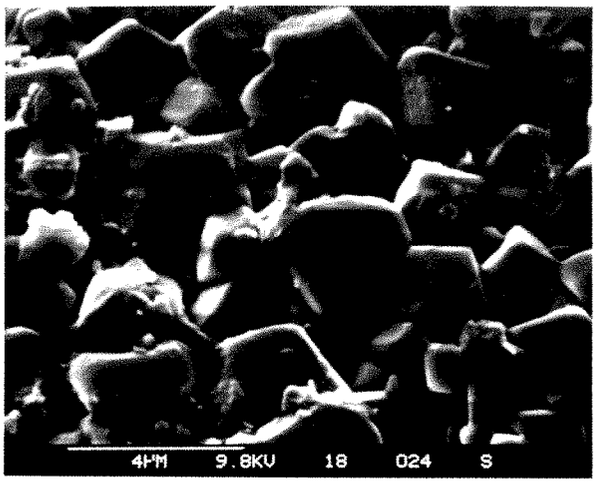

Fig: 2·10

with t = 0 to 0.4 were obtained and shown in Fig. 2.11 to 2.15, and the diffraction maxima were indexed with the method as explained elsewhere and were checked and tallied with those expected, for spinel structure. The reflections for cubic structure are (111), (220), (311), (222), (400),(422), (333) and (444) etc. These planes are allowed for cubic spinel structure. The d-values of the samples are represented in the diffractograms of respective samples.The calculated d-values of the samples are in close agreement with the observed d-values which clearly indicates that the ferrites prepared are fully formed with spinel structure. The lattice parameter (a) was determined for different compositions of the system and represented in the table No. 2.2.

TABLE 2.2

THE VALUES OF LATTICE CONSTANTS, X-RAY DENSITIES AND R_A and R_B

Compositions	lattice constant A^o	R_A	R_B	X-ray density gram/cc
$Cd_{0.3}Ni_{0.7}Fe_2O_4$	8.4608	1.9197	2.0644	5.496
$Cd_{0.3}Ni_{0.75}Mn_{0.05}Fe_{1.9}O_4$	8.4451	1.916	2.606	5.529
$Cd_{0.3}Ni_{0.8}Mn_{0.1}Fe_{1.8}O_4$	8.4546	1.918	2.0629	5.5127
$Cd_{0.3}Ni_{0.9}Mn_{0.2}Fe_{1.6}O_4$	8.4480	1.9168	2.0613	5.530
$Cd_{0.3}Ni_1Mn_{0.3}Fe_{1.4}O_4$	8.4565	1.918	2.0633	5.5173

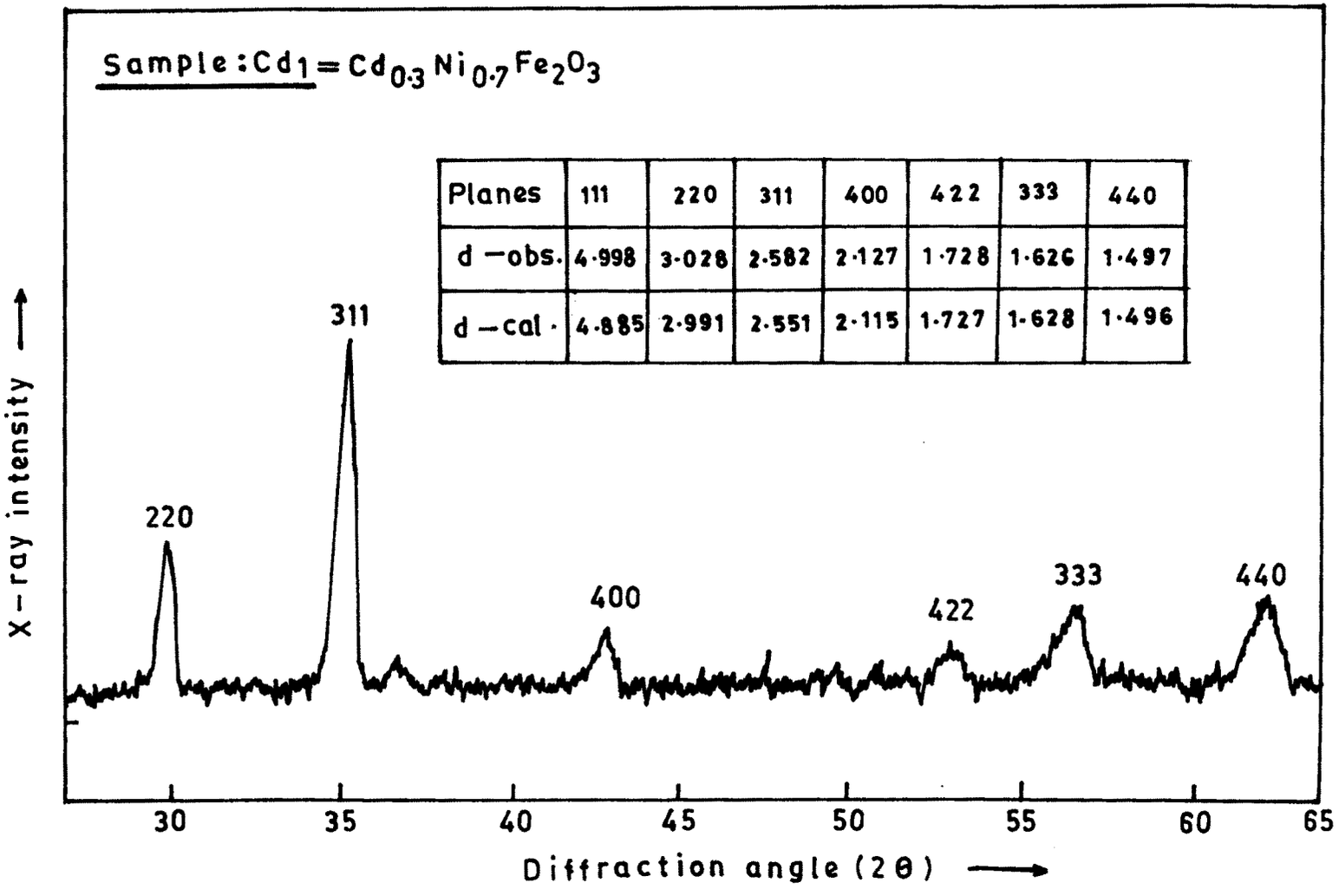
Sample : $Cd_1 = Cd_{0.3}Ni_{0.7}Fe_2O_3$
Planes | 111 | 220 | 311 | 400 | 422 | 333 | 440
d –obs. | 4·998 | 3·028 | 2·582 | 2·127 | 1·728 | 1·626 | 1·497
d –cal. | 4·885 | 2·991 | 2·551 | 2·115 | 1·727 | 1·628 | 1·496
X-ray intensity
220
311
400
422
333
440
30
35
40
45
50
55
60
65
Diffraction angle (2θ)

FIG. 2·11

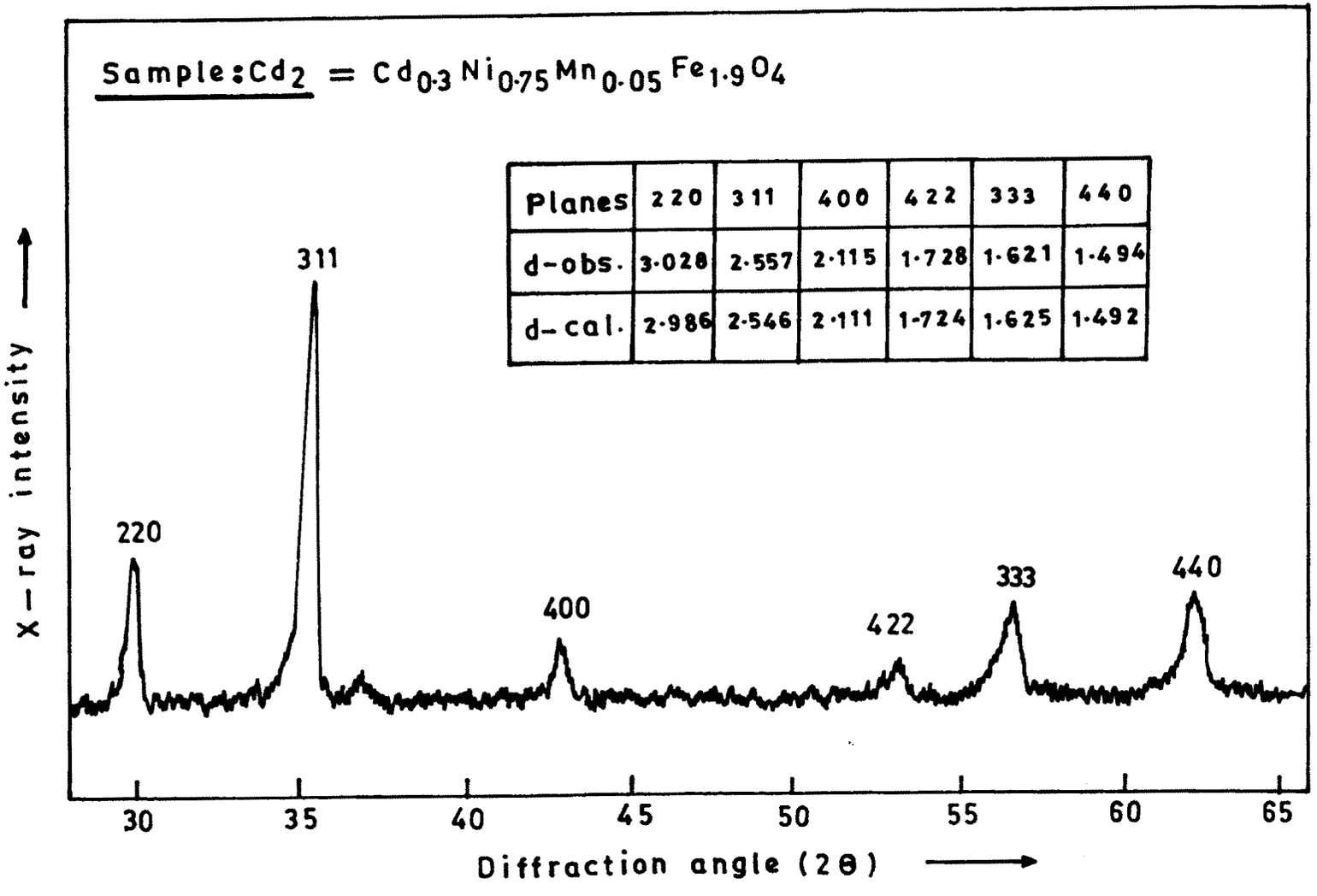
Sample:Cd2 = Cd0·3 Ni0·75 Mn0·05 Fe1·9 O4
Planes 220 311 400 422 333 440
d-obs. 3·028 2·557 2·115 1·728 1·621 1·494
d-cal. 2·986 2·546 2·111 1·724 1·625 1·492
X-ray intensity
220
311
400
422
333
440
30
35
40
45
50
55
60
65
Diffraction angle (2θ)

FIG. 2·12

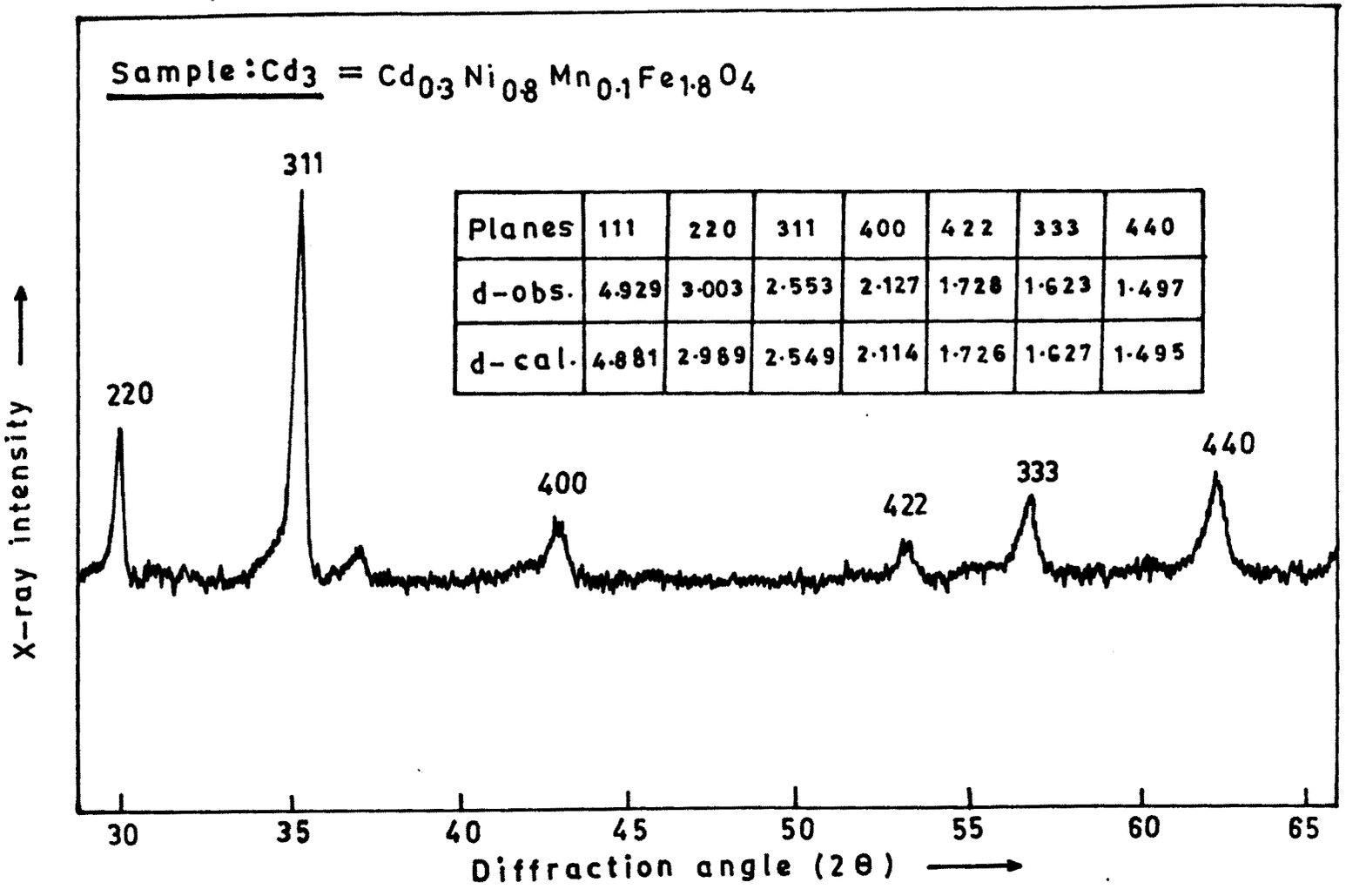

Planes	111	220	311	400	422	333	440
d-obs.	4·929	3·003	2·553	2·127	1·728	1·623	1·497
d-cal.	4·881	2·989	2·549	2·114	1·726	1·627	1·495

FIG. 2·13

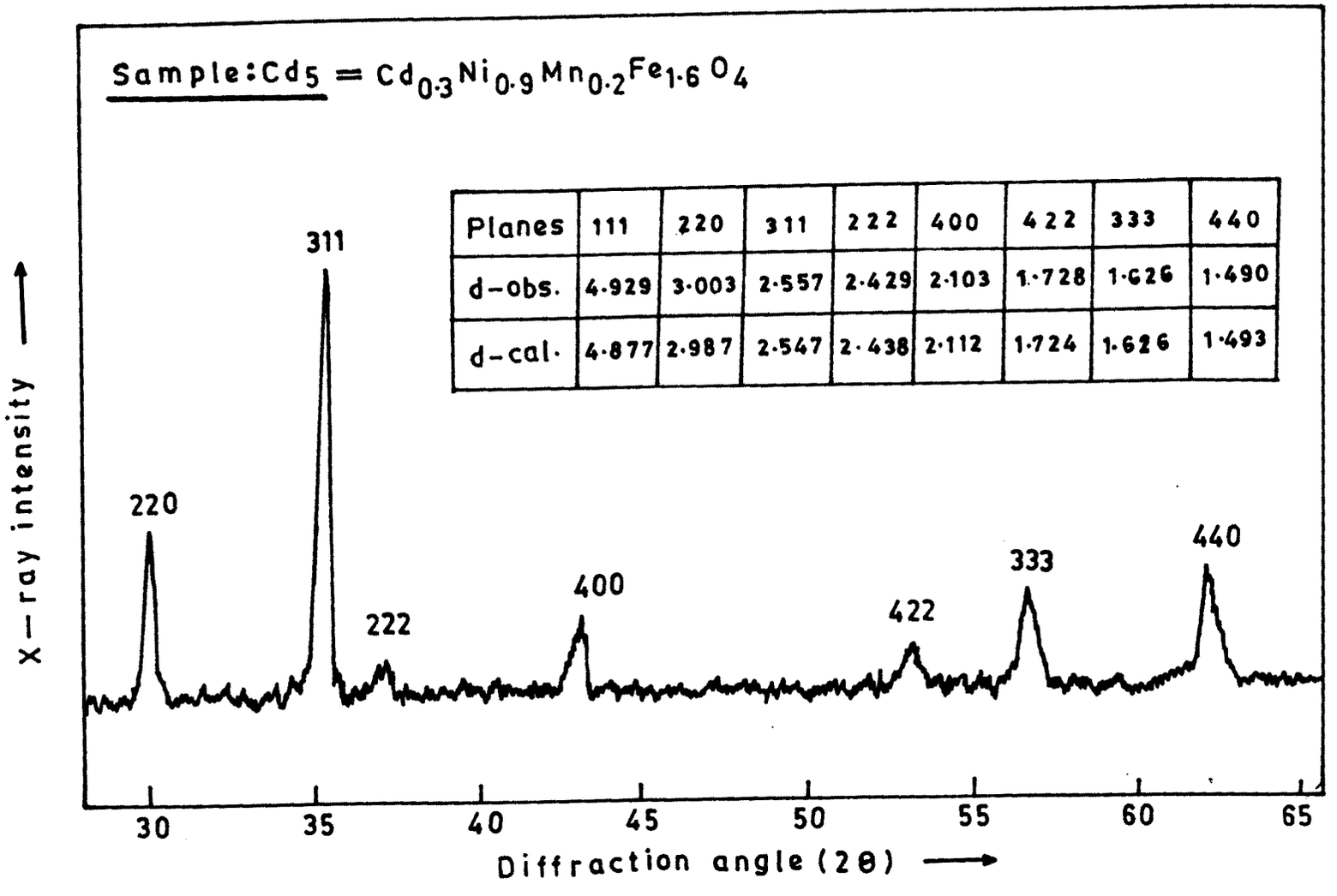
Sample:Cd5 = $Cd_{0.3}Ni_{0.9}Mn_{0.2}Fe_{1.6}O_4$
Planes | 111 | 220 | 311 | 222 | 400 | 422 | 333 | 440
d-obs. | 4.929 | 3.003 | 2.557 | 2.429 | 2.103 | 1.728 | 1.626 | 1.490
d-cal. | 4.877 | 2.987 | 2.547 | 2.438 | 2.112 | 1.724 | 1.626 | 1.493
311
220
222
400
422
333
440
X-ray intensity
30
35
40
45
50
55
60
65
Diffraction angle (2θ)

FIG. 2.14

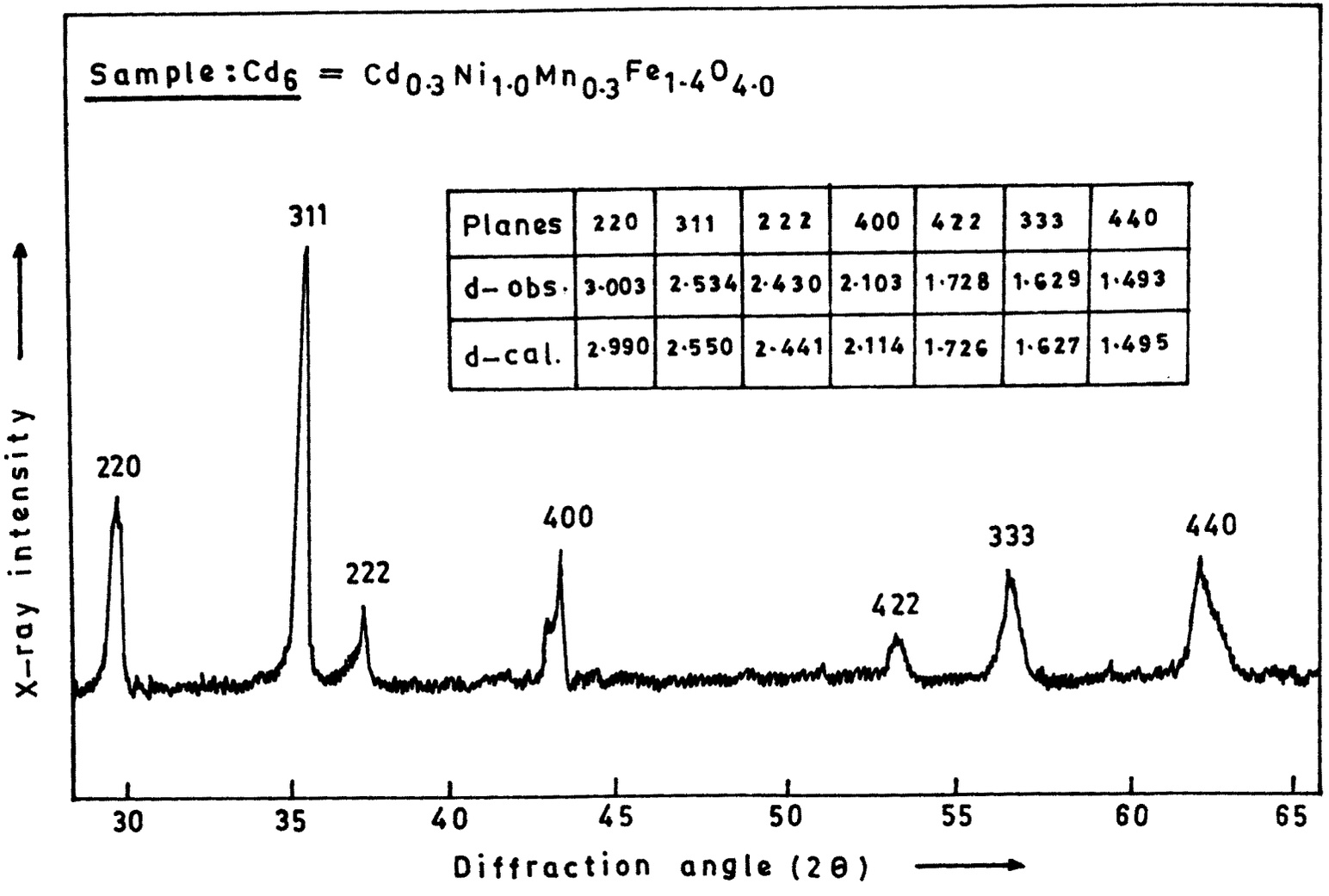
Sample : Cd_6 = $Cd_{0.3}Ni_{1.0}Mn_{0.3}Fe_{1.4}O_{4.0}$
Planes | 220 | 311 | 222 | 400 | 422 | 333 | 440
d-obs. | 3.003 | 2.534 | 2.430 | 2.103 | 1.728 | 1.629 | 1.493
d-cal. | 2.990 | 2.550 | 2.441 | 2.114 | 1.726 | 1.627 | 1.495
220
311
222
400
422
333
440
X-ray intensity
30
35
40
45
50
55
60
65
Diffraction angle (2θ)

FIG. 2.15

From the table it is observed that the lattice constant variation is not in a systematic way with increase of 't'. The calculated values of R_A and R_B are also shown in Table 2.2.

The variation of lattice constant with ionic radias has been explained in Ni-Cd, Cu - Zn ferrites. The ionic radii of Ni^{2+}, Fe^{3+} are 0.72, 0.6, and 0.64 respectively. In our system iron is replaced by the relation.

$$2Fe^{3+} \rightarrow Ni^{2+} + Mn^{4+} \qquad .....(2.25)$$

Secondly the variation of lattice constant with the substitution of tetravalent ions like Ti, Zr, was discussed by A.R. Das[17] et al in Ni -Zn ferrites and Zr in Cu - Zn ferrite by S.R. Jadhav[18] et al . The effect of substitution of tetravalent ion on lattice constant (a) can be explained on the basis of combined effect of cation size 'b' on the repulsion parameter and of the A-site charge on the Madelung constant (M), where the lattice parameter is proportional to $(b/M)^{1/9}$.

The spinel system (Fe_3O_4,—Mn_3O_4) have studied by D.G. Wickham[19]He has observed that the cubic lattice constant remains the same for the intermediate compositions, where Mn^{3+} is replacing by Fe^{3+} on the octahedral site. Octahedrally co-ordinated Mn^{3+} appear to have almost identical ionic radii in the oxides.

Lattice constant for the system,

$Mn_{2-x}Fe_xO_3$ (α Mn_2O_3 structure[20]) have been reported to show no change with concentration of Mn. Considering the above facts

the variation in the lattice constant may be only due to Nickel ions, but we have not observed systematic variations in the lattice constant. This may be due to the combined effect of Mn and Ni with respect to Fe and may be due to composition of MnO_2 i.e.

$$4MnO_2 \rightarrow 2Mn_2O_3 + O_2 \uparrow \qquad .....(2.26)$$

which may be cause to change the ionic charge in spinel lattice.

2.15 (b) SEM :

The SEM micrograph of the samples are presented in the Fig. 25 to 2.10 for the present series. The important features of the micrographs are given.

1. The sample Cd_1 reveals large size grains. The sample Cd_1 which is undoped "Mn" having higher permeability (μ) and higher porosity.
2. For the samples $Cd_2$and Cd_3 the grain size decreases where as Cd_4, Cd_5 and Cd_6 the grain size increases. The samples Cd_2,Cd_3 Cd_4 shows fine grain structure with less porosity.
3. The $Cd_5$and Cd_6 samples shows more porosity.

The segragation off impurity phases have not been observed clearly in all the samples.

The grain growth kinetics for Mn-Zn and Ni-Zn ferrites prepared by ceramic technique with substituents like SiO_2,GeO_2,P_2O_5 have been studied by the group at NPL[21]. They have

concluded that, upto solid solubility limit the grains grow normally as decided by oxygen ion vacancy concentration. discontineous grain growth with lot of intra-granular porosity occurs and at higher concentrations the grains again becomes regular with a few intra-granular pores and a second phase present at grain boundaries and corners. The similar behaviour of normal grain growth is observed except for undoped samples in our case. The exaggerated grain growth and intra-grannular pores are not observed. This is because in our sample no second phase has been observed upto t = 0.4, 'Mn' content which is also confirmed by X-ray diffraction technique, where as no extra lines have been observed. This itself indicates that, the samples formed are with single phase solid solution.

The properties such as permeability, losses are mostly dependent on the microstructural condition. Effect of grain size, porosity and imperfections on permeability are discussed by A. Goldman.[22] Effect of grain size on permeability was made by Ross on Mn - Zn ferrite[23] and Guillaud and Polous[24] on Ni - Zn ferrites. They have observed the increase in ' μ ' with increase of grain diameter, but this is not true, because graiin size alone is not an important factor for high μ . Other imperfections limiting the movement of domain wall are also the pores.

From Figure (2,16) it is observed that the permeability decreases with decrease of grain size upto t = 0.15 and again the μ decreases contineously, where as grain size increases. Guillaud[25] showed in Ni - Zn ferrites that although the permeability increased

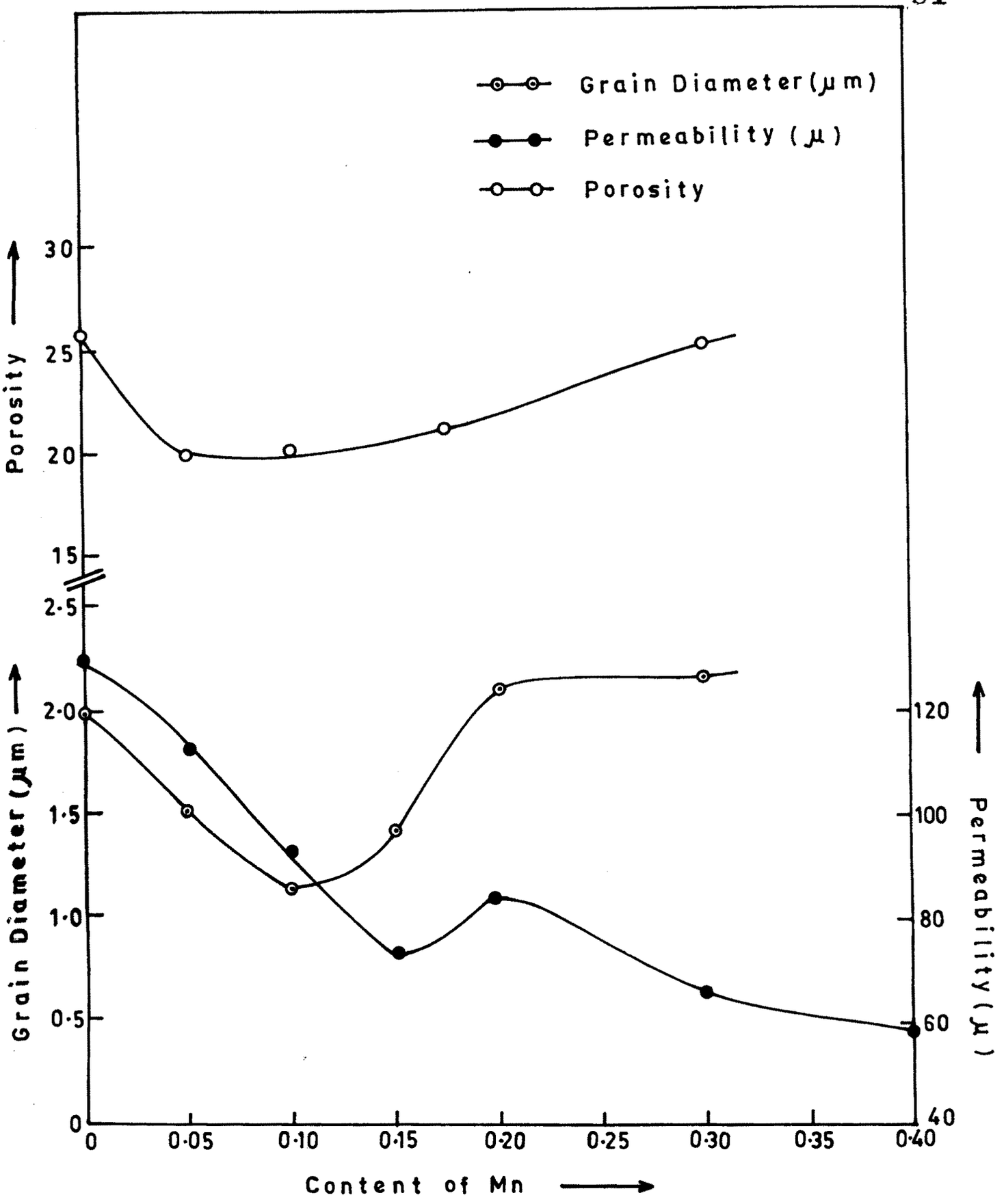

FIG. 2·16 — VARIATION OF GRAIN DIAMETER(μm), PERMEABILITY(μ), AND POROSITY WITH CONTENT OF Mn.

with grain size upto 15 μm, it decreases there after and this decrease was due to included porosity. Ross et al[23] have found that an increase in ' μ ' with grain size is primarily caused by decrease in internal stresses in the material, but this is true only when the crystalline anisotropy is very low. In the regions, where this anisotropy has a finite value, the permeability (μ) can even then decrease with increase of grain diameter.

The Globus has given the relation as,

$$\mu_i = \frac{M_s^2 \, dm}{k_1} \qquad \text{.....(2.27)}$$

where K = is anisotropy constant

dm = is grain diameter

M_s = is saturation magntisation

So dependiing on the value of K_1 the ' μ ' changes. Generally any disturbance by inclusions, pores, inhomogeneties or an excessively large number of grain boundaries will decrease the permeability. All factors are valied but no relation has put forward to relate microstructural parameters e.g. internal strain, grain size, pore size and pore density quantitatively to permeability.[26]

REFERENCES

1. K.J. Standley, 'Oxide magnetic materials' Chap 2. P.9 Clearendon Press New York (1972).
2. Economus G.J., Ame. Cera Soc. 38, 241 (1955)
3. Wolf W.P., Rodrigue G.P., J.Appl. Phys. 29, 105 (1958).
4. Sato T, IEEE Trans. Mag. 6, 798 (1970).
5. Sato T, Kuroda C., Saito M., Ferrites Proc. Int. Conf. Kyoto Tokyo Press P. 72, (1970).
6. Guillaud, C., Paulus M.C.R., Acad. Sci. 242, 2525-8 (1956).
7. Heister W.J., Phy. Appl. 30, 225 (1959).
8. Perduijn D.J. and Peloschek H.P., Proc-Brit. Ceram. Soc. Vo.10, 263 (1968).
9. Kamazin A.S., Fiz. Tuerd Tela (USSR) 17, 2419 (1975).
10. Zener C.See Smith C.S., Trans. AIME 175, 15 (1948).
11. Reijnen P.J.L., Science of ceramics 4, 169 (1968).
12. C.Kittle, 'Introduction to Solid State Physics' 5th Edi. John Wiely and Sons Inc. N.Y. (1976).
13. B.D. Cullity, 'Element of X-ray diffraction' Addision Wesley Publishing Co.Inc. England (1959).
14. P.Debye and P.Scherrer, Physick Z. 17, 277 (1916) and 18, 219 (1917).
15. A.N.Hull, Phys. Rev. 9, 84, 564 (1916) and 10, 661(1917).
16. Henry, N.F.M., Lipson H. and Wooster W.A., 'The interpretation of X-ray diffraction photographs' Macmillan and Co.Ltd., London (1961).

17. A.R.Das, V.S. Ananthan and D.C.Khan, J.Appl. Phys. 57(1), 4189 (15th April 1985).

18. s.R.Jadhav, S.R. Sawant, S.S. Suryavanshi, S.A.Patil and R.N.Patil, ICF-5, India P. 453 (1989). Kolhapur 416004 India.

19. D.G.Wickham, J.Inorg. Nucl. Chem. Vol.33, PP 313-320, (1969).

20 S.Geller, R.W. Grant, J.A. Cape and G.D. Espinosa, J.Appl. Phys. 38, 1457 (1967).

21. i) Jain G.C., Das B.K. and Kumaris, J.Appl. Phy. 49, 2894, (1978).

ii) Jain G.C., Das B.K. and Kumaris, IEEE, Trans. On Mag-mag-12, 1428 (1980).

22. A Goldman, Ekectronic ceramics Properties , Devices and applications edited by Lionel. M. Levinson Marcell Dekker Inc. N.Y. P147, (1988).

23. C.Ross, I.Hanke and Emser, Z-Angew Phy.17, 504 (1964).

24. Guillaud, C. Polous M; C.R. Acad. Sci-242, 2525-8(1956).

25. Guillaud, Proc. IEEE, 104B, 165 (1957).

26 A.L.Stuijts, ceramic microstructures and their analysis, significance and production Edi. Richard M, Fulrath Joseph A. Pask John Willey and Sons N.Y. (1968) P.443.